Contact-angle hysteresis on periodic microtextured surfaces: Strongly corrugated liquid interfaces

Stanimir Iliev* and Nina Pesheva†
Institute of Mechanics, Bulgarian Academy of Sciences, Acad. G. Bonchev St. 4, 1113 Sofia, Bulgaria
(Received 12 October 2015; revised manuscript received 31 May 2016; published 20 June 2016)

We study numerically the shapes of a liquid meniscus in contact with ultrahydrophobic pillar surfaces in Cassie's wetting regime, when the surface is covered with identical and periodically distributed micropillars. Using the full capillary model we obtain the advancing and the receding equilibrium meniscus shapes when the cross-sections of the pillars are both of square and circular shapes, for a broad interval of pillar concentrations. The bending of the liquid interface in the area between the pillars is studied in the framework of the full capillary model and compared to the results of the heterogeneous approximation model. The contact angle hysteresis is obtained when the three-phase contact line is located on one row (block case) or several rows (kink case) of pillars. It is found that the contact angle hysteresis is proportional to the line fraction of the contact line on pillars tops in the block case and to the surface fraction for pillar concentrations 0.1–0.5 in the kink case. The contact angle hysteresis does not depend on the shape (circular or square) of the pillars cross-section. The expression for the proportionality of the receding contact angle to the line fraction [Raj *et al.*, Langmuir **28**, 15777 (2012)] in the case of block depinning is theoretically substantiated through the capillary force, acting on the solid plate at the meniscus contact line.

DOI: 10.1103/PhysRevE.93.062801

I. INTRODUCTION

The creation of micropillars on solid surface can enhance the hydrophobicity of the surface and also can decrease the hysteresis of the contact angle (CA) when the surface is in contact with liquids [1]. These properties arise when the contact of the liquid with the solid surface takes place only at the tops of the pillars. The conditions for the appearance of this wetting regime, known as Cassie's, composite, or fakir state, and its wetting properties are studied intensively for the case of identical and periodically distributed pillars [2]. However, the dependence of the advancing CA θ^a (ACA), the receding CA θ^r (RCA), as well as their difference, defined as the CA hysteresis (CAH), on the pillars shape and size, the intrapillar distance, the orientation of the liquid front with respect to the pillar structure, etc., are still not sufficiently well elucidated. The most extensively studied case is that of periodically distributed pillars of circular and square cross-sections. Experimental [3–15] and numerical data [13,14,16–22], in this case, point to certain universality of the ACA, whose cosine is ≈ -1, while the value of the RCA depends on the parameters of the rough surface. This feature of the CAH is known as the asymmetry of the CAH. Arguments are given [23] that the reason for the asymmetry of the hysteresis is that the contact lines (CLs), corresponding to the ACA and the RCA—the advancing contact line L^a (ACL) and the receding contact line L^r (RCL), respectively—have different activation energies. Nevertheless, this approach needs more elaborate research, since numerical studies for chemical defects [24,25] find that in some cases of randomly distributed defects there is no asymmetry of the CAH.

It is not sufficiently clear whether and how the RCA can be expressed as a function on the parameters of the liquid front and the structure of the pillars. The Joanny and de Gennes model [26], as well as other theoretical studies [27,28], lead to a linear dependence of the $\cos\theta^r$ on the pillars surface fraction p, i.e., the ratio between the contact area on the tops of the pillars and the total projected area, while the experimental data does not uniquely support this finding. Linear dependence on p is obtained in the interval [0.05,0.15] [28] and also in the interval [0.05,0.8] [4,9]; however, other experiments show that for small $p \in [0.02,0.08]$ [6] and for big variation of $p \in [0.05,0.45]$ [7] and $p \in [0.05,0.8]$ [29], a deviation from the linear dependence is observed. Reyssat and Quéré [7] give an explanation of the deviation from the linear dependence, using the approach of Joanny and de Gennes, by taking into account the influence of the energy, related to the CL corrugation, due to the CL pining and depinning as a whole (i.e., block case; see Ref. [14]). They obtained that

$$\cos\theta^r \sim p\ln(1/p), \tag{1}$$

however, the exact determination of the proportionality coefficient is still pending. In another approach [30], the RCA is determined through the chemical heterogeneity approximation of the problem [19], using the modified Cassie equation and introducing the fraction λ_l of the pillars material along the CL length. However, it is not easy to obtain the fraction λ_l, since in order to do that, one needs to know *a priori* the shape of the CL. In this case, when the three-phase CL is located on one row of pillars, an approximation of the fraction λ_l through the line fraction ϕ was suggested [10,14,16,31], where ϕ is defined as the ratio of the pillar size to the cell size λ along the horizontal line connecting pillars centers (i.e., $\phi = a/\lambda$ when the pillars cross-section is a square of size a and $\phi = d/\lambda$ when the pillar cross-section is a circle of diameter d). For systems, for which it is assumed that the material of the pillars is homogeneous and the liquid makes with it a unique equilibrium CA $\theta_{\rm eq}$, the modified Cassie equation for the RCA θ^r takes the following form:

$$\cos\theta^r = \phi\cos\theta_{\rm eq} + (1-\phi). \tag{2}$$

*stani@imbm.bas.bg
†nina@imbm.bas.bg

 ©2016 American Physical Society

The experimental data [6,10,16,32] show that the RCA is well fitted by Eq. (2); however, this equation is derived under certain assumptions for the RCLs, which are not supported completely by the experimental data and the numerical simulations. For example, in Refs. [7] (Fig. 4), [29] (Fig. 2), and [31] (Fig. 3) it is assumed that the RCL is stuck only to the defect borders, while the experimental data [15,32–34] and the numerical simulations [19,20] find that the RCL passes also through the inner part of the defects. Also in Ref. [19], through numerical simulation the drop RCL was obtained (see Fig. 7(a) in Ref. [19]), indicating a tendency of the drop to "ball up" in those areas where it is not in contact with the solid surface, which does not agree with the assumptions, from which Eq. (2) follows. All of the above imply that a more precise study and analysis of this relation is highly needed.

Equation (2) has a limited validity, since the assumptions made for its derivation are not always fulfilled, since in reality the CL is not always located on a single row of pillars. When the CL has parts on several rows of pillars, it is possible a kink type of CL-receding to occur [10,13,14]. It is shown that in this case, for pillars of circular [13,14] and of square [10] cross-section, the RCA is different from the angle predicted by Eq. (2). A type of Eq. (1) dependence for $p \in [0.02,0.08]$ and linear dependence for $p \in [0.08,0.24]$ of the RCA on p are found experimentally and numerically (by the help of the public software Surface Evolver [35]) in the case of pillars of circular cross section [13,14]. On the other hand, a numerical study of the RCA [16] on a drop's CL for $p = 0.44$ in the case of pillars of square cross section, forming square lattice, using again the Surface Evolver [35], finds a value in agreement with Eq. (2); however, one has to bear in mind that in this case the drop's CL is not located on a single row of pillars. Therefore, a more precise study is needed on the influence of the kink-type CL receding on the value of the RCA for different pillar cross sections and concentrations p.

The main goal of this work is to obtain numerically the shapes of the advancing and receding liquid meniscuses in contact with solid surfaces, covered with identical and periodically distributed micropillars in Cassie's wetting regime, when the respective CLs are located on one or several rows of pillars of circular and square cross-sections. The dependence of the CAH on the pillar surface concentration p and line fraction ϕ will be obtained and analyzed in a broad interval of these quantities.

II. PROBLEM DESCRIPTION

We study here the capillary rise at a vertical plate in a tank of liquid (see Fig. 1), used quite often for the determination of the static CA. The relation between the averaged macroscopic CA $\langle\theta\rangle$ and the averaged capillary rise height $\langle h\rangle$ of the liquid meniscus is used for the determination of the CA [20,24,25,36],

$$\langle\theta\rangle = \arcsin\left(1 - \rho g\langle h\rangle^2/2\gamma\right), \tag{3}$$

where ρ is the difference of the densities of the liquid in the tank and the ambient fluid, g is the gravity acceleration (in a study of capillary rise the effect of gravitation cannot be ignored), and γ is the surface tension of the liquid free surface Σ. More specifically, we focus here on the meniscus-free surface Σ,

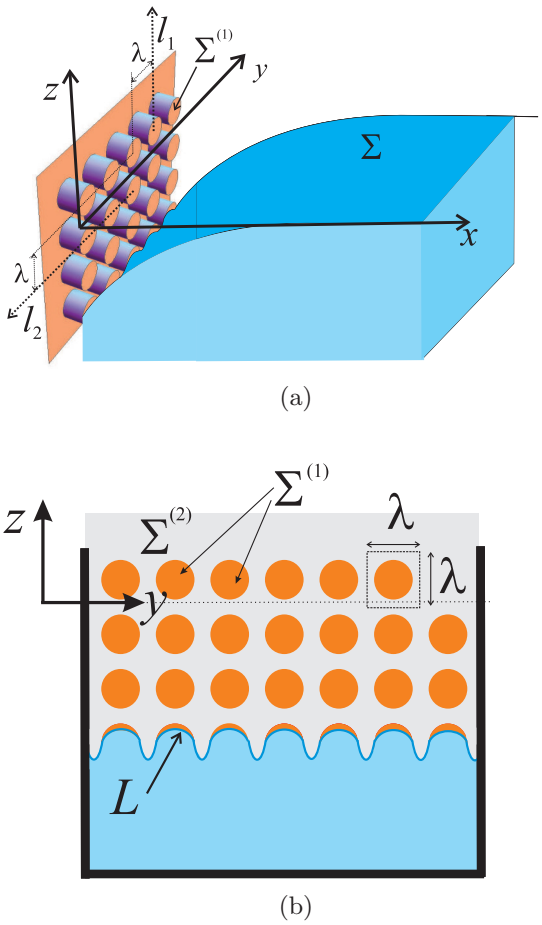

FIG. 1. Schematic drawing of (a) the considered model system and (b) the heterogeneous surface of the plate in Cassie's wetting regime.

forming when a vertical hydrophobic microstructured rough solid plate is partially immersed in a tank of liquid as illustrated in Fig. 1. The plate surface is covered by micropillars, whose cross-section is either a square or a circle. We use the coordinate system, depicted in Fig. 1, where the $\vec{y}$ axis is horizontal and the $\vec{z}$ axis is directed upwards. In this coordinate system, the tops of the pillars lie in the plane $\{x = 0\}$. The pillars form a square lattice with spatial period λ, such that $\lambda \ll l_c$, where l_c is the capillary length, defined as usual as $l_c = \sqrt{\gamma/\rho g}$. For pillars with square cross-section, it is assumed as customary, that the sides of the squares are parallel to the vectors $\vec{l}_1$, $\vec{l}_2$ ($\vec{l}_1 \perp \vec{l}_2$), characterizing the square lattice. Note that the liquid front is always perpendicular to the $\vec{z}$ axis.

We assume here that the liquid meniscus wets the rough solid surface in Cassie's (or composite) regime [1]. In this case the liquid is in contact only with part of pillars tops, forming the liquid-solid contact area $\Sigma_{ls} \subset \Sigma^{(1)}$ (the surface $\Sigma^{(1)}$ is composed of all pillars tops). We obtain in this work the static RCA and ACA in the same way as they are determined in the experimental measurements in such systems, i.e., by fixing the vertical position of the defect pattern on the plate with respect to the liquid level far from the plate, after having moved the plate upward and downward into the liquid pool until CL depinning starts to occur.

Full capillary model (FCM). The metastable meniscus states are determined through minimization of the free energy U of the system [37]

$$U = \gamma \int_{\Sigma} d\Sigma - \gamma \int_{\Sigma_{ls}} \cos\theta_{eq}\, d\Sigma + \rho g \int_{\Omega} z\, d\Omega, \qquad (4)$$

where Ω is the volume of the liquid in the pool.

Heterogeneous approximation model (HAM). In this case the problem of obtaining solutions in Cassie's wetting regime reduces to the special case of finding the equilibrium state of a liquid meniscus in contact with a vertical chemically heterogeneous flat plate, consisting of two kinds of domains $\Sigma^{(1)}$ and $\Sigma^{(2)}$ of different wettability with sharp borders between them [19]. The domain $\Sigma^{(1)}$ is composed of the surface of the pillars tops. The air, filling the crevices between the micropillars, forms the domain $\Sigma^{(2)}$, which is characterized by an equilibrium CA of 180°. Thus, the equilibrium meniscus states are determined by finding the minima of the following expression of the free energy:

$$U = \gamma \int_{\Sigma} d\Sigma - \gamma \int_{\Sigma^{(1)}} \cos\theta_{eq}\, d\Sigma + \gamma \int_{\Sigma^{(2)}} d\Sigma + \rho g \int_{\Omega} z\, d\Omega. \qquad (5)$$

For the points of the CL, which are located on the borders between the defects, the equilibrium CA has value between θ_{eq} and 180° (for details, see Ref. [38]).

We obtain the equilibrium meniscus shapes numerically in the interval $y \in [0, l_y]$, where the value of l_y and the periodic boundary conditions depend on the initial shape of the meniscus and on the relative position of the liquid meniscus and the pillars lattice. We employ a minimization algorithm to obtain the metastable equilibrium meniscus. Several previous studies, involving finding the metastable equilibrium meniscus states with free energy Eq. (4) or Eq. (5), are obtained also numerically using similar minimization algorithm. In many of these, the public domain software Surface Evolver [35], the Local Variations algorithm [39], and the Hybrid Energy-Minimization method [40] are used. Most of these studies concern the equilibrium shape of a drop, and some are devoted to the Wilhelmy plate geometry; however, most of them are employing the heterogeneous approximation [9,20,25,41]. Here, we employ the minimization algorithm, described in detail in Refs. [41,42]. Since, as customary, we assume here that the tank dimensions are much bigger than l_c, which allows us to apply the 3D minimization algorithm only in a part of the coordinate space, close to the CL as in Ref. [25]. Similar to the study in Ref. [25], we will use the method of matching, sufficiently away from the plate, the numerical solution for the meniscus shape with the analytical solution, available for meniscus with symmetric in y—direction meniscus shape (i.e., the shape for a liquid meniscus in contact with a homogeneous plate).

III. RESULTS

We present here results for water meniscus, studied experimentally in Ref. [15] in contact with micropillars, forming square lattice, where pillars cross-section is a circle with diameter $d = 18$ μm and the equilibrium contact angle of the liquid meniscus with the pillar's material is $\theta_{eq} = 90°, 98°, 110°$. In addition to that, we also study the case when the pillars cross-section is a square of size $a = 18$ μm.

A. The CL is located on a single horizontal row of pillars (block depinning case)

In this case we obtain periodical solutions for the liquid meniscus in the interval $y \in [0,\lambda]$. By the help of the numerical method we obtain the equilibrium receding and advancing shapes of the liquid meniscus (which are used to determine the RCA and the ACA) for different values of the pillar concentration p. We also simulate numerically immersing and withdrawing plates to find the equilibrium meniscus shapes with CLs situated between the RCL and the ACL.

The obtained solutions, determining the RCA, are shown in Fig. 2 in a neighborhood of the CL, for a system with $\theta_{eq} = 98°$, where the pillars cross-section is circle and the pillar concentration is $p = 0.28$ as in Fig. 5 in Ref. [15] and Fig. 2 in Ref. [34]. In Fig. 2(a) the solution of the full model is presented and in Fig. 2(b) for comparison the solution of the heterogeneous approximation model is shown. The shapes of the two meniscus solutions are identical in a neighborhood of the CL and are also quite similar to the shape, shown in Ref [15] (see Fig. 5 there), found for the same values of pillars diameter d and concentration p, but slightly different values of CA θ_{eq} and surface tension γ. One can see from Fig. 2, that the RCLs, found in the frameworks of the two models, pass through the same row of pillars (of the same height) and therefore one gets the same values of the RCA in both models. The value of the RCA, obtained through Eq. (3), is 119.2°, which is very close to the value found using Eq. (2), 119.08°.

Our numerical studies of the equilibrium meniscus shapes and the RCLs for pillar line fractions $\phi \in [0.22,0.95]$ (or surface concentrations $p \in [0.05,0.9]$ for square and $p \in [0.04,0.7]$ for circular pillar cross section) indicate that the RCA is well approximated by the relation Eq. (2) for both pillars of circular and square cross sections. Note that one has $\phi = \sqrt{p}$, in the case of pillars of square cross section; $\phi = 2\sqrt{p/\pi}$, in the case of circular pillar cross section; note also that for $p > \pi/4$ the circles overlap and the pattern topology changes. However, for concentrations $p \leqslant 0.1$, the heterogeneous approximation model is no longer applicable, since during the minimization process a self-intersection of the CL occurs. Within the limits of its applicability the obtained solutions of the RCA are the same as the results of the full model.

The occurrence of self-intersection of the CL is an indication that for small pillar concentration the receding meniscus surface is not well approximated by a flat surface in the area between the pillars, though the mean curvature of the meniscus is small in the regions between the pillars (more precisely, the surface curvatures in this area in y and z directions are big but of opposite signs). This explanation is supported by the simulation results. We present our results for the meniscus shape, found by employing the full capillary model, in Fig. 3 in a neighborhood of the RCL at pillar concentration $p = 0.05$. The meniscus shape and, respectively, the CL, are strongly corrugated at $p = 0.05$ for the chosen values of the parameters. Only one period in the horizontal (y direction) is shown so that the bending of the liquid interface is clearly visible. One can observe the presence of a noticeable "bridge" in the z direction

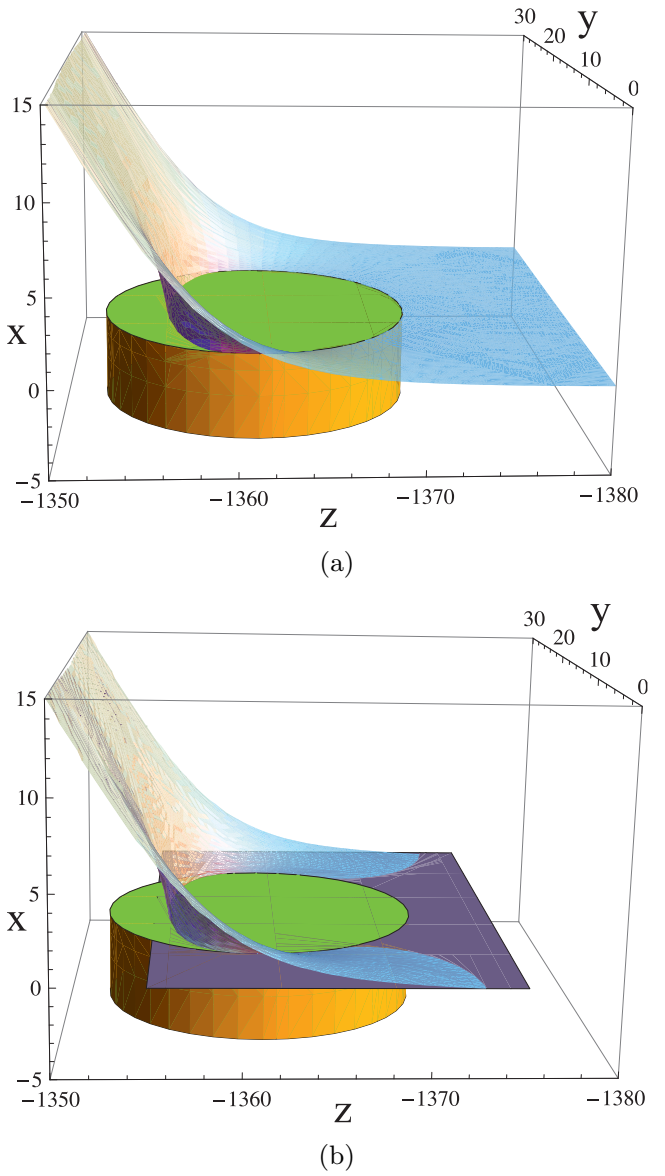

FIG. 2. Meniscus solutions, used to determine the RCA, are shown in a neighborhood of the CL, at pillar concentration $p = 0.28$ and $\theta_{eq} = 98^\circ$, when the pillars cross-section is a circle: (a) solution of the full model; (b) solution of the heterogeneous approximation model.

between the two neighbor posts, due to the significant value of the curvature in this direction.

This effect persists also at higher pillar concentrations, see, e.g., the meniscus shape shown in Fig. 2 at $p = 0.28$; however, the effect is weaker and is observable only in the close vicinity of the pillars, where the CL is located. Similar behavior of the meniscus, before the depinning of the CL from the pillars, is observed in Refs. [34,43].

We would like to point out here that the equilibrium meniscus states depend also on the relative position in the vertical direction of the pillar lattice (or, respectively, of the plate) with respect to the liquid level far from the plate, which can be characterized by the height of the centers of the pillar tops. Due to that, the RCA can be determined also by averaging of the averaged heights of the RCLs (i.e., the CL of the highest

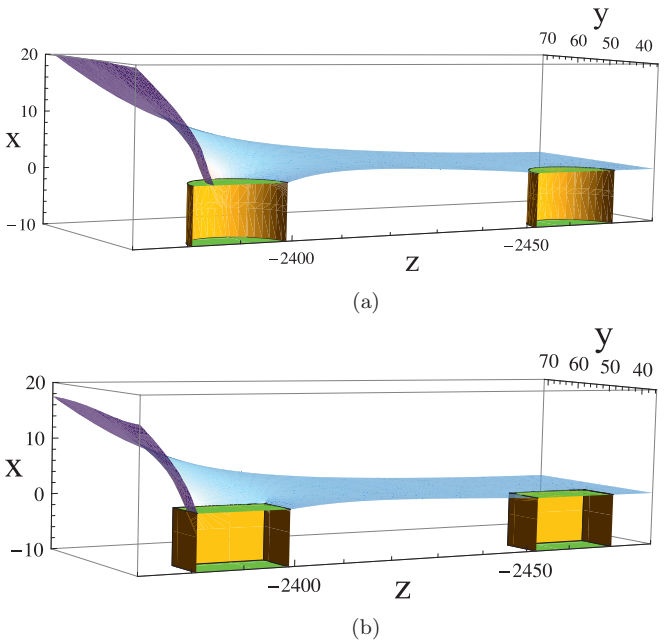

FIG. 3. Meniscus solutions, obtained by employing the full capillary model, are shown in a neighborhood of the RCL, at pillar concentration $p = 0.05$ and $\theta_{eq} = 98^\circ$ when the pillars cross-section is (a) circle and (b) square.

averaged height at fixed lattice position) over all different lattice positions [20]. Therefore, one needs to determine the CLs with the highest averaged heights at different relative positions of the pillar lattice with respect to the liquid. Our numerical results show that for concentrations $p \in [0.05,0.7]$, in the case of circular pillar tops, all such RCLs have parts, which are inner for the pillar tops [as seen in Fig. 2(a)]. In this case, when the pillar cross-section is square, we find that the respective RCLs (found at different plate positions) have different locations on the pillar's top—see Fig. 4, where several equilibrium RCLs are presented of the meniscus solutions at pillar concentration $p = 0.25$. They are obtained by employing the heterogeneous approximation model and are presented in the reference system of the rough plate, where one period of the lattice is shown. Among these, only the CL, which is adhering to the vertical side of the square defect (bold line), is stable with respect to small variations of the lattice vertical position.

Our numerical results show that every horizontal row of defects, whose centers are at height between the height of the RCL and $-l_c\sqrt{2}$, is in contact with only one metastable equilibrium state. In the case of pillars with circular cross section, where the equilibrium CLs located a few periods λ below the RCL, also have parts that are inner for the pillars tops, similar to the RCL. The equilibrium CLs of smaller average heights are in contact only with the upper border of the circular defects. In the case of pillars of square cross section, all equilibrium CLs, except for a part of the CL of the highest averaged height, are in contact with the upper border of the square. The ACA is determined through the height of the CL, located closest to the limiting height $-l_c\sqrt{2}$. For the ACL one has

$$\langle h(\mathrm{ACL})\rangle - l_c\sqrt{2} < \lambda\,. \tag{6}$$

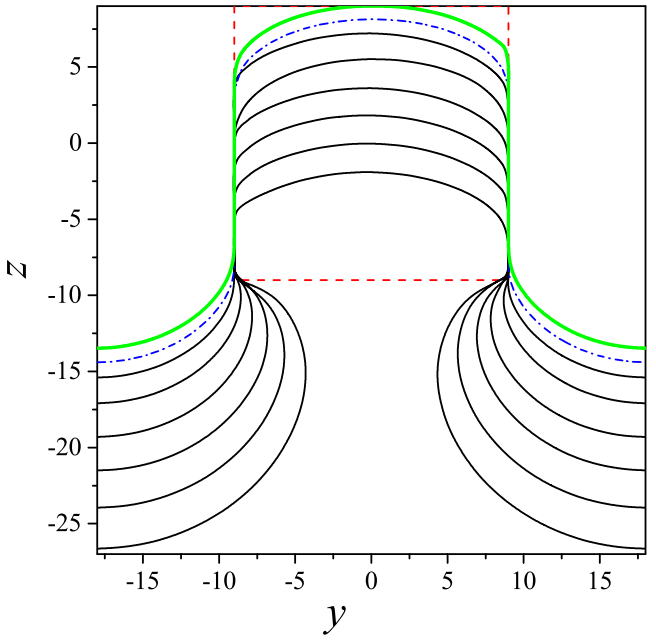

FIG. 4. Set of RCLs at different vertical positions of the pillar lattice with respect to the liquid level far from the plate at pillar concentration $p = 0.25$ and $\theta_{eq} = 98^\circ$ in the case, when the pillar's cross section is a square.

The ACA has a value close to 180°, and when the period λ is decreasing it approaches fast 180°.

For the system under study, there exists a relation between the averaged CA $\langle\theta\rangle$ and the averaged CL height $\langle h\rangle$, and there is also a relation between the averaged CL height $\langle h\rangle$ and the vertical component of the capillary force, exerted by the liquid on the solid plate [20]. When the CL of the equilibrium liquid meniscus is in contact with only one horizontal row of pillars, every equilibrium meniscus state with CA $\langle\theta\rangle$ generates on the plate a capillary force, smaller than or equal to the capillary force in the only equilibrium state with CL L^s of the same system; however, in contact with a heterogeneous plate, whose surface consists of alternating vertical stripes of widths a and $\lambda - a$ (where $a = d$) with equilibrium CAs θ_{eq} and 180°, respectively, and line fraction along the y direction of $\phi = a/\lambda$ and $1 - \phi$. Thus, one has

$$\langle\theta\rangle \leqslant \theta^C , \tag{7}$$

where θ^C is Cassie's angle for the system in contact with the heterogeneous plate, whose surface consists of alternating vertical stripes:

$$\cos\theta^C = \phi\cos\theta_{eq} - (1 - \phi) . \tag{8}$$

Thus from Eqs. (7) and (3) it follows that the average height of the RCL is smaller than or equal to the average height of the CL L^s. In addition to that, note that when the minimization algorithm is started with an initial meniscus, whose CL is a straight horizontal line, passing through the centers of the circular or square pillars' tops, during the minimization process the CL will try naturally to approach the CL L^s. When the initial CL lies outside the defect, it has the tendency to move in the direction toward the only equilibrium state of the homogeneous state with CA 180°, i.e., its height approaches the limit $-l_c\sqrt{2}$. These two features imply that at every horizontal row of pillars with center height between L^s and $-l_c\sqrt{2}$ there is one equilibrium CL. Therefore, the RCL for the considered system is always located either on the row of pillars, where the CL L^s is positioned, or on the first row below L^s. When $\lambda \ll 1$, one finds that the RCA $\approx \theta^C$. In the case of pillars with a square cross section, the RCL can actually coincide with the CL L^s. This is illustrated in Fig. 4, where the equilibrium CL is presented by the dash-dotted line, since in this case this CL obviously satisfies the conditions for equilibrium, when the liquid is in contact with the solid surface of alternating vertical stripes and where the square is a part of such stripe and has the appropriate height.

B. Triple line with a kink

We find numerically also the equilibrium shapes of the liquid meniscus, corresponding to the RCA and the ACA, for a broad interval of values of the pillars surface concentration p, when the triple line is located on more than one row of pillars, so that a kink appears.

1. The CL is located on two horizontal consecutive rows of pillars

We assume here that the meniscus CL is periodic along the y axis with period $l_y = 2n\lambda$ and along this interval it is in contact with total of $2n$ pillars. The first n pillars are located on one row and the next n pillars are located on the next lower row of pillars. We note that in the case of pillars of circular cross section, the pillars' concentration $p < 0.25$ and $n \gg 1$ is studied in detail in Refs. [13,14]. A part of the meniscus solution of the full model for $n = 10$ (also exhibiting strong corrugation) in a neighborhood of the triple line kink that we obtained is shown in Fig. 5. The solution is obtained at pillars concentration $p = 0.28$—the case considered experimentally in Ref. [34]. One can see that there is a good agreement of the numerically obtained meniscus shape with the one observed by scanning electron microscopy, presented in Fig. 2 in Ref. [34]. We find that the value of the RCA does not change when the CL is located on more than eight consecutive pillars tops on the same row. Our numerical results indicate that the values of the RCA and the ACA, found in the frameworks of the full model and the heterogeneous approximation model, do not differ. However, the application of heterogeneous approximation model is restricted to pillar concentrations $p > 0.2$. In a neighborhood of the triple line kink, the curvature of the liquid interface, in the area between the neighboring pillars, is more pronounced than in the block depinning case. This can be clearly observed by comparing the meniscus solution for the RCA, shown in Fig. 6 at $p = 0.05$, with the meniscus solution for the RCA in the block depinning case at the same concentration, displayed in Fig. 4(b).

The effective adhesion, defined as $1 + \cos\theta^r$ (see Ref. [14]), of the obtained meniscus solutions for $\theta_{eq} = 98^\circ$, is shown in Fig. 7 (solid circles) as function of the surface concentration p in the interval [0.05,0.65] for pillars with circular cross-section. Our numerical results show that the same dependence also holds for pillars with square cross section. One can see that the results for the effective adhesion are fitted in the interval [0.1,0.5] very well by a linear function

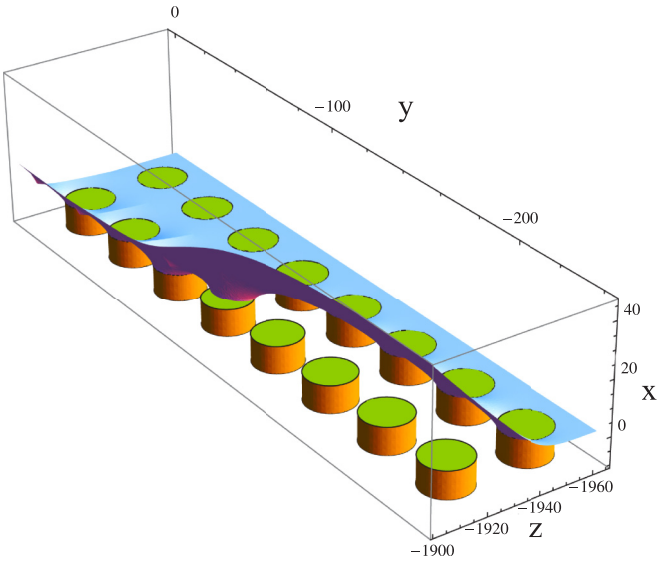

(a)

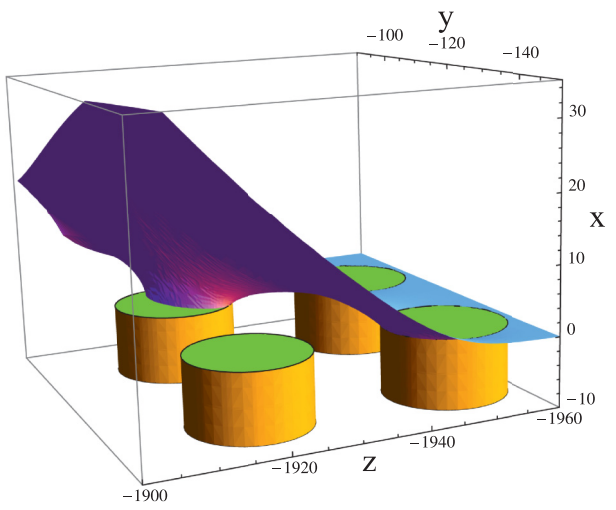

(b)

FIG. 5. (a) Part of the liquid meniscus in a neighborhood of the triple line kink at $p = 0.28$ and $\theta_{eq} = 98^\circ$ in the case of pillars with circular cross section. (b) Enlarged image of the meniscus in Fig. 5(a) where the kink occurs.

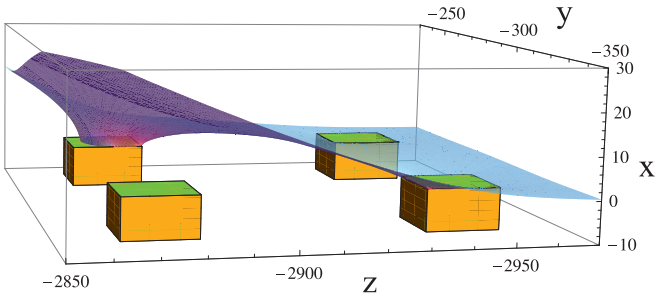

FIG. 6. Meniscus solution, for the RCA, obtained by employing the FCM at pillar concentration $p = 0.05$ and $\theta_{eq} = 98^\circ$, when pillars cross section is a square.

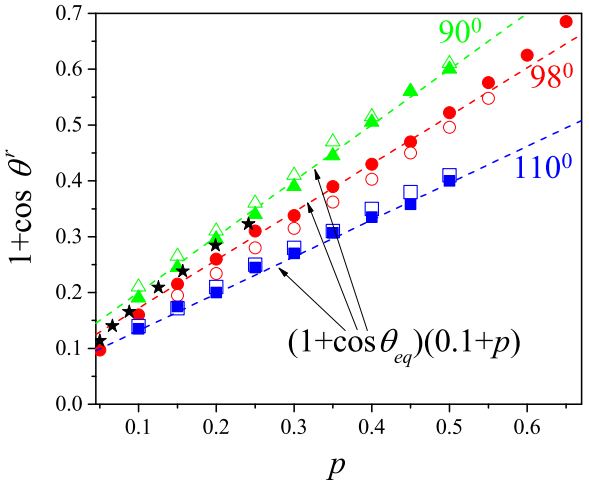

FIG. 7. The effective adhesion $1 + \cos\theta^r$ of the obtained meniscus solutions as function of the pillar surface concentration p for pillars with circular cross section when the CL has a kink for $\theta_{eq} = 90^\circ$ (triangles), $\theta_{eq} = 98^\circ$ (circles), and $\theta_{eq} = 110^\circ$ (squares): the solid symbols are the results for the case in Sec. III B 1. (horizontal pillar lattice); the empty symbols are results for the case considered in Sec. III B 2. (rotated pillar lattice). The stars are the numerical results from Ref. [14]. The dashed lines are the respective fits by Eq. (9).

of p:

$$1 + \cos\theta^r = \big(1 + \cos\theta_{eq}\big)(0.1 + p), \tag{9}$$

shown by the dashed line in Fig. 7. For lower concentrations $p < 0.1$ and for higher concentrations $p > 0.5$ the effective adhesion deviates from the linear dependence and approaches fast 0 and $1 + \cos\theta_{eq}$, respectively. These results are in a good agreement with the numerical results, found in Ref. [14] for concentrations p in the interval [0.02, 0.24] and $\theta_{eq} = 90^\circ$ (shown in Fig. 7 by solid stars) in the case of pillars of circular cross section. Our numerical calculations, performed also for $\theta_{eq} = 90^\circ$ and $\theta_{eq} = 110^\circ$ (shown in Fig. 7 by solid triangles and solid squares, respectively) indicate that Eq. (9) (shown by the dashed lines in Fig. 7) holds in the interval [0.1, 0.5] for other values of the equilibrium CA.

2. *The CL is located on several nonhorizontal rows of pillars*

The CL can be located on pillars tops belonging to several different rows when the pillars lattice vectors $\vec{l}_1$, $\vec{l}_2$, defining its orientation, are not parallel to the $\vec{y}$, $\vec{z}$ axes. Here, we demonstrate this for pillars with circular cross section, when the square lattice of pillars is rotated at angle φ around the origin, such that $\tan\varphi = 1/m$, leading to a defect lattice, characterized by vectors $\vec{l}_1 = (m,1)$; $\vec{l}_2 = (-1,m)$. Then along the y axis, one has lattice with period $l_y = \lambda\sqrt{m^2+1}$. By the help of the numerical algorithm we obtain the receding and the advancing equilibrium shapes of the liquid meniscus within the heterogeneous approximation model for two rotations of the lattice, characterized by $m = 2,3$ and pillar concentrations $p \in [0.15,0.55]$. The obtained RCLs at pillar concentration $p = 0.25$ and $\theta_{eq} = 98^\circ$ are shown in Fig. 8 for two rotations of the pillar lattice: $m = 2\varphi = \tan^{-1}(1/2)$ ($\varphi \approx 26.6^\circ$) in (a) and $m = 3$ $\varphi = tan^{-1}(1/3)$ ($\varphi \approx 18.4^\circ$) in (b).

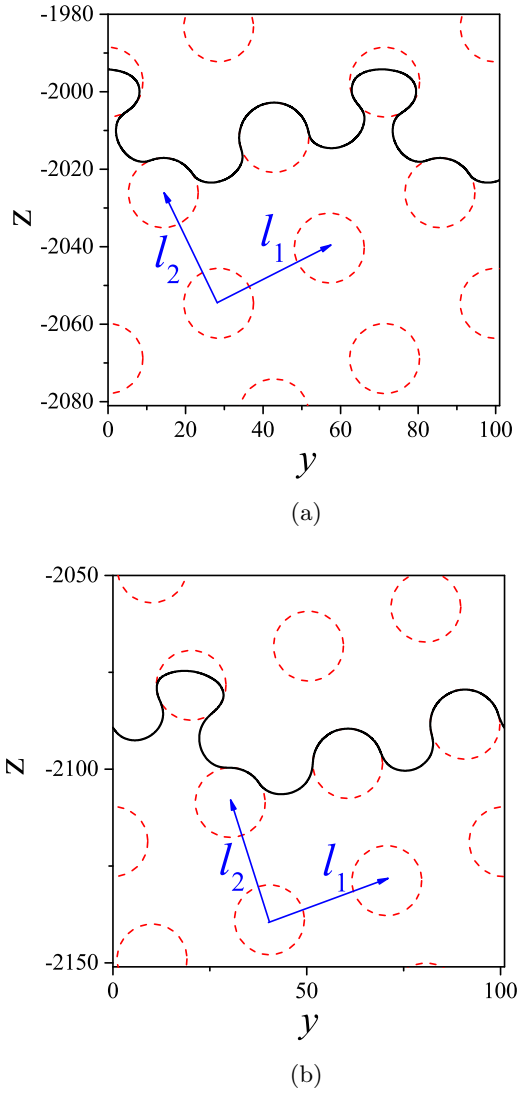

FIG. 8. CLs of the highest averaged height (RCLs), when $p = 0.25$ and $\theta_{eq} = 98^\circ$, along the y axis in the case of a rotated with respect to the liquid level pillar lattice at: (a) $\varphi \approx 26.6^\circ (m = 2)$ and (b) $\varphi \approx 18.4^\circ$ $(m = 3)$.

The obtained results for the RCA when the lattice is rotated at $\varphi = \tan^{-1}(1/3)$ are shown in Fig. 7 for $\theta_{eq} = 90^\circ, 98^\circ, 110^\circ$ with open triangles, circles, and squares, respectively. One can see that at fixed concentration p, the effective adhesion $1 + \cos\theta^r$ has values, which are approximately by 0.03 lower than its values for the case, considered in Sec. III B 1. We find that the RCA for the case $m = 2$ is between the values of the RCA for $m = 3$ and of the RCA, when the CL with a kink is located on two consecutive rows (the case studied in Sec. III B 1). Based on these results, for pillars with circular cross section, one can conclude that, when the triple line has a kink, the RCA depends weakly on the orientation of the pillar lattice with respect to the liquid level far from the plate. This conclusion is checked for $\theta_{eq} \in [90^\circ, 110^\circ]$. One finds also that in this case (i.e., triple line with a kink), the ACA is close to 180°.

IV. CONCLUSION

The CAH was studied for a liquid in contact with ultrahydrophobic pillar surfaces (characterized by $\theta_{eq} \in [90^\circ, 110^\circ]$) in Cassie's wetting regime. The meniscus shapes were found both by the full capillary model and by the heterogeneous approximation model for a broad interval of values of pillar concentration p for micropillars of both square and circular shapes of the pillars cross section. One can clearly observe the curving of the liquid interface in the vicinity of the CL in the framework of the full capillary model. The limits of applicability of the heterogeneous approximation model were determined. It was found that the CLs and, respectively, the apparent CAs can effectively be determined by both methods for not very small pillar concentrations; however, for smaller pillar concentrations, a "bridge" forms in the direction of the liquid front between two neighboring posts, which can only be obtained in the framework of the full capillary model. This clearly indicates that the heterogeneous approximation model is inapplicable at these concentrations.

Our numerical results show that in both cases, square and circular cross sections of the pillars, one finds the same values of the RCA and ACA for a broad interval of pillars surface concentrations p or line fractions ϕ, whereas the type of the concentration (surface p or line ϕ) one should use in the description of the results depends on whether the CL has a kink or not. More precisely, in the case of a CL with a kink the effective adhesion is a linear function of the pillar surface concentration p in the interval $(0.1 - 0.5)$. For lower $p < 0.1$ and higher $p > 0.5$ concentrations the effective adhesion deviates from the linear dependence and approaches fast 0 and $1 + \cos_{eq}$, respectively. In the case of CL without a kink (block case) the effective adhesion is a linear function of the pillar line fraction ϕ in the whole interval of considered fractions. The coefficient of proportionality in both linear functions depends on the equilibrium CA. In all considered cases the ACA is always close to 180°.

For pillars of circular cross section, the RCA depends weakly on the orientation of the liquid front with respect to the pillars lattice (i.e., when the CL has a kink), while the case of pillars of square cross section is more complex.

The performed study and the conclusions drawn contribute to a better understanding of the mechanism of wetting of rough solid surfaces and can help the design of new superhydrophobic surfaces.

[1] D. Quéré, Annu. Rev. Mater. Res. **38**, 71 (2008).
[2] L. Barbieri, E. Wagner, and P. Hoffmann, Langmuir **23**, 1723 (2007).
[3] D. Öner and T. J. McCarthy, Langmuir **16**, 7777 (2000).
[4] C. Priest, T. W. J. Albrecht, R. Sedev, and J. Ralston, Langmuir **25**, 5655 (2009).
[5] C. Priest, R. Sedev, and J. Ralston, Phys. Rev. Lett. **99**, 026103 (2007).

[6] A. L. Dubov, J. Teisseire, and E. Barthel, Europhys. Lett. **97**, 26003 (2012).
[7] M. Reyssat and D. Quéré, J. Phys. Chem. B **113**, 3906 (2009).
[8] K. Y. Yeh, L. J. Chen, and J. Y. Chang, Langmuir **24**, 245 (2008).
[9] Y. Kwon, S. Choi, N. Anantharaju, J. Lee, M. V. Panchagnula, and N. A. Patankar, Langmuir **26**, 17528 (2010).
[10] C. Dorrer and J. Rühe, Langmuir **22**, 7652 (2006).
[11] K. M. Smyth, A. T. Paxson, H.-M. Kwon, and K. K. Varanasi, Surface Innovations **1**, 84 (2012).
[12] A. Gauthier, M. Rivetti, J. Teisseire, and E. Barthel, Langmuir **30**, 1544 (2014).
[13] A. Gauthier, M. Rivetti, J. Teisseire, and E. Barthel, Phys. Rev. Lett. **110**, 046101 (2013).
[14] M. Rivetti, J. Teisseire, and E. Barthel, Phys. Rev. Lett. **115**, 016101 (2015).
[15] R. Dufour, M. Harnois, V. Thomy, R. Boukherroub, and V. Senez, Soft Matter **7**, 9380 (2011).
[16] W. Choi, A. Tuteja, J. M. Mabry, R. E. Cohen, and G. H. McKinley, J. Colloid Interface Sci. **339**, 208 (2009).
[17] B. M. Mognetti and J. M. Yeomans, Langmuir **26**, 18162 (2010).
[18] D. Chatain, D. Lewis, J. P. Baland, and W. C. Carter, Langmuir **22**, 4237 (2006).
[19] C. Dorrer and J. Rühe, Langmuir **23**, 3179 (2007).
[20] S. Iliev, N. Pesheva, and V. S. Nikolayev, Phys. Rev. E **90**, 012406 (2014).
[21] H. Kusumaatmaja and J. M. Yeomans, Langmuir **23**, 6019 (2007).
[22] N. Anantharaju, M. V. Panchagnula, and S. Vedantam, Langmuir **25**, 7410 (2009).
[23] L. Gao and T. J. McCarthy, Langmuir **22**, 6234 (2006).
[24] R. David and A. W. Neumann, Langmuir **26**, 13256 (2010).
[25] D. Iliev, N. Pesheva, and S. Iliev, Langmuir **29**, 5781 (2013).
[26] J. F. Joanny and P. G. de Gennes, J. Chem. Phys. **81**, 552 (1984).
[27] N. A. Patankar, Langmuir **26**, 7498 (2010).
[28] Y. Xiu, L. Zhu, D. W. Hess, and C. P. Wong, J. Phys. Chem. C **112**, 11403 (2008).
[29] R. Dufour, M. Harnois, Y. Coffinier, V. Thomy, R. Boukherroub, and V. Senez, Langmuir **26**, 17242 (2010).
[30] C. Extrand, Langmuir **18**, 7991 (2002).
[31] R. Raj, R. Enright, Y. Zhu, S. Adera, and E. N. Wang, Langmuir **28**, 15777 (2012).
[32] S. T. Larsen and R. Taboryski, Langmuir **25**, 1282 (2009).
[33] D. Chatain, C. Lesueur, and J.-P. Baland, Langmuir **22**, 4230 (2006).
[34] R. Dufour, P. Brunet, M. Harnois, R. Boukherroub, V. Thomy, and V. Senez, Small **8**, 1229 (2012).
[35] K. Brakke, Exp. Math. **1**, 141 (1992).
[36] A. W. Adamson and A. P. Gast, *Physical Chemistry of Surfaces* (Wiley, New York, 1997).
[37] L. D. Landau and E. M. Lifshitz, *Fluid Mechanics* (Pergamon Press, Oxford, 1987).
[38] S. Iliev and N. Pesheva, Langmuir **19**, 9923 (2003).
[39] S. Iliev, On one modification of the local variations method, Moscow State University Vestnik, Series 15: Computational Mathematics and Cybernetics 4, pp. 55–60 (1991) (in Russian), http://maik.ru/cgi-perl/journal.pl?lang=eng&name=cmatcmgu.
[40] H. Matsui, Y. Noda, and T. Hasegawa, Langmuir **28**, 15450 (2012).
[41] S. Iliev, Comput. Methods Appl. Mech. Engrg. **126**, 251 (1995).
[42] S. Iliev, N. Pesheva, and V. S. Nikolayev, Phys. Rev. E **78**, 021605 (2008).
[43] F. Schellenberger, N. Encinas, D. Vollmer, and H.-J. Butt, Phys. Rev. Lett. **116**, 096101 (2016).